

Cite this: *Chem. Sci.*, 2014, 5, 4196

A general approach to mono- and bimetallic organometallic nanoparticles†

Sudheendran Mavila, Illya Rozenberg and N. Gabriel Lemcoff*

A comprehensive methodology to prepare nanometric size organometallic particles (ONPs) containing rhodium(I), iridium(I) and nickel(0) with ROMP-derived polycycloocta-1,5-diene (pCOD) by a controlled single chain collapse mechanism was developed. The polymeric complexes could be produced *via* direct exchange of the respective labile ligands of metal complexes by the 1,5-hexadiene elements in pCOD, or *via in situ* reduction of metal ions in the presence of the polymer. These well-defined π -bound polymeric complexes were characterized by UV-Vis spectroscopy, dynamic light scattering (DLS) and size exclusion chromatography (SEC) measurements and the resulting polymer sizes were found to be inversely proportional to the amount of metal added due to concomitant single chain collapse. Moreover, these procedures were readily extended to the synthesis of organobimetallic nanoparticles containing two metals; which could be added in commutative order and specific metal ratios. The embedded metal elements were found to be readily accessible for applications in catalysis, where the close proximity of the catalytic centers led to distinctive reactivity compared to the isolated complexes.

Received 29th April 2014

Accepted 18th June 2014

DOI: 10.1039/c4sc01231c

www.rsc.org/chemicalscience

Introduction

The advancement of polymer science embraces the invention of molecular constructs that provide functional applications. As a result, the development of novel methodologies for the production of polymers and complex macromolecular architectures^{1–6} stands out as an appealing goal enthusiastically pursued by the synthetic chemistry community. In this regard, metallopolymers offer a great advantage, as they may combine the catalytic/functional properties of the metal complex with the material/structural facets of polymers. Polymers containing metals may be classified by the type of ligand used to bind the metal, by the type of metal used to dope the polymer, or by the way the metal is bound to the polymer chain (*i.e.* as a metallic substituent in the side chain, or a main chain metal polymer; linear, dendritic or star-shaped architectures; dynamic or static binding modes, *etc.*).⁷ Even though they have been known for more than three decades,^{8,9} only since the mid-1990s have techniques that allow the synthesis and characterization of well-defined metallopolymers been mature enough to be practically useful. Modern metallopolymers are used for a great variety of applications, including catalysis, sensing, OLED constituents, optics, information storage, and even stimuli-responsive materials.¹⁰ For example, in emissive layers, the introduction of iridium into the polymer allows phosphorescence

emission, dramatically enhancing the quantum yield,¹¹ and metallocsupramolecular polymers have been used to make special materials with the ability to heal themselves after sustaining damage.¹² Recently, Gladysz *et al.* ingeniously polymerized an η^4 -benzene iridium complex, taking advantage of the uncoordinated double bond of the benzene ring.¹³ This methodology afforded an unprecedented polyacetylene framework where iridium atoms were bound along the butadiene fragments of the main chain. Another recent example from the Manners group¹⁴ shows how by simply changing the reaction conditions a ring-opening reaction of a methylsilaferrocenophane affords very different polymers. Thus, the creation of a new metallopolymer family and its correct characterization can lead to accurate structure–activity relationship studies and to the design of more complex and useful materials. Well-defined polymer bound complexes may be also used as soluble polymer supported catalysts under homogeneous conditions.^{15–17} In general, these polymer bound catalysts may be recovered and reused by precipitating them in a poor polymer solvent.¹⁸ In this context, complexes of rhodium and iridium have received considerable attention because of their large potential to carry out various organic transformations with high degrees of stereo- and regio-selectivity.^{19,20}

An attractive process to regulate the physical properties of macromolecules is by their transformation to well-defined organic nanoparticles by intramolecular cross-linking. Three main approaches stand out as the most common methods to induce chain collapse in polymers; irreversible covalent, reversible covalent (dynamic) or non-covalent cross-linking.²¹ The strategies for chain collapse can also be classified according to the type of chemistry used to generate the nanoparticle.²² The

Department of Chemistry, Ben-Gurion University of the Negev, Beer-Sheva 84105, Israel. E-mail: lemcoff@bgu.ac.il

† Electronic supplementary information (ESI) available: Detailed experimental procedures and characterization of ONPs including: ¹H and ¹³C NMR, SEC spectra and GC-MS chromatograms of reaction mixtures. See DOI: 10.1039/c4sc01231c

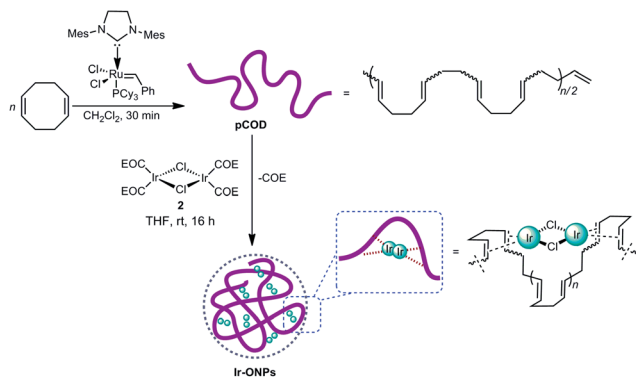
first examples of intramolecular cross-linking date back forty years to the seminal work by Walsh *et al.*²³ Martin continued the study of intramolecularly cross-linked polymers, both experimentally and theoretically, in the early 1980s²⁴ and demonstrated the relationship between the cross-link density and the contraction factor. The field laid more or less dormant for the next 20 years, until the turn of the century where new chemistries were developed for cross-linking strategies, such as the benzocyclobutane (BCB) method²⁵ and olefin metathesis,^{26,27} among others. [For recent examples of intramolecularly cross-linked polymers and dendrimers see ref. 28–31.]

Herein, we introduce a wide-ranging strategy for the exploitation of organometallic bonds to induce single chain collapse of ROMP derived pCOD. Thus, rhodium, iridium and nickel organometallic nanoparticles were made and characterized. In addition, we disclose that this strategy may be used to form nanoparticles containing both rhodium and iridium ions in any chosen ratio. Moreover, as a proof of concept and to detail the potential of these materials, we show how the catalytic properties of the embedded metal may be transformed by changing the architecture of the organometallic nanoparticle.

Results and discussions

Synthesis of organometallic nanoparticles of iridium(I)

Having recently disclosed a convenient and straightforward synthesis of pCOD complexes of rhodium(I) by using



Scheme 1 Schematic illustration of the preparation of Ir-ONPs.

[RhCl(C₂H₄)₂]₂ (**1**) as a precursor cross-linker,³² we set out to determine the generality of this concept by extending it to other metals and bimetallic structures. Thus, single chain collapse of pCOD was attempted *via* the intramolecular binding of 1,5-hexadiene fragments to iridium(I) under dilute conditions.

In order to obtain an understanding of the exchange process, the model monomers 1,5-cyclooctadiene (COD), 1,5-hexadiene and (perhaps as a more realistic framework) a mixture of 4,8-dodecadienes were mixed with [IrCl(COE)₂]₂ (**2**) (the tetrakis-ethylene complex of iridium was unstable and could not be used for this purpose). The facile exchange process afforded compounds **3**, **4** and **5**, as confirmed by NMR spectroscopy (see the ESI†).

Having shown that the model dienes readily exchanged the COE ligands in **2**,³³ this complex was tested as a cross-linker for pCOD. Indeed, pCOD ($M_n \approx 50\,000\text{ g mol}^{-1}$, PDI = 1.02) quickly reacted with **2** (10 mol% with respect to the 1,5-diene unit) in THF and exchanged COE at room temperature to afford Ir-ONPs (Scheme 1).

The appearance of a new broad signal at $\delta = 4.56\text{--}4.72$ ppm corresponding to olefin protons bound to an iridium metal center in the ¹H NMR spectrum strongly supported the formation of Ir-ONPs *via* the exchange of COE by 1,5-hexadiene units (Fig. S16, ESI†). In addition, we sought a more practical method to monitor the formation of ONPs and decided to probe UV-Vis spectroscopy. Pleasingly, the resulting Ir-ONPs showed an absorption maximum at 446 nm, similar to that observed for the COD complex (**3**) (451 nm) (Fig. 1c),³⁴ while the absorption maximum seen for complex **2** at 420 nm disappeared; strongly supporting the occurrence of binding events of 1,5-hexadiene units to Ir(I). UV measurements were also extended to the Rh-ONPs with similarly positive results (*vide infra*). Finally, the most compelling evidence for the formation of well-defined organometallic nanoparticles of iridium was acquired by measuring the size of the polymer obtained after adding the metal. The SEC overlay of Ir-ONPs produced by using 10 and 2 mol% of **2** (with respect to 1,5-hexadiene units of pCOD) together with the starting polymer material provides compelling evidence for a well-controlled single chain collapse (Fig. 1a), indicating an almost 30% decrease in hydrodynamic radius according to the triple-detector system used.³⁵ Supporting the notion that chelation is the main driving force behind the single

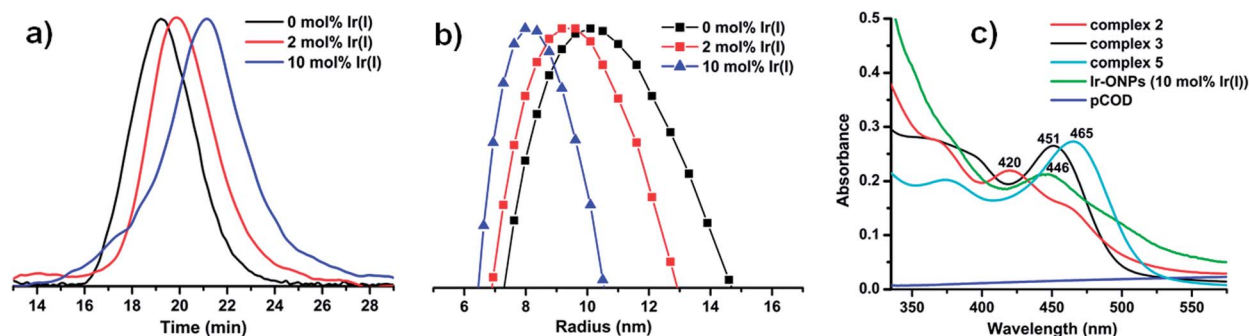


Fig. 1 (a) Overlay of the SEC traces obtained for Ir-ONPs at varying concentrations of Ir(I) and pCOD. (b) Overlay of DLS traces obtained for Ir-ONPs at varying concentrations of Ir(I) and pCOD. (c) UV-Vis spectra of pCOD, **2**, **3**, **5** and Ir-ONPs (10 mol% Ir(I)).

Table 1 SEC and DLS measurements of Ir-ONPs with varying iridium content^a

Entry	Ir(I) ^b [mol%]	M _n ^c [$\times 10^4$ g mol ⁻¹]	PDI	R _g ^c [nm]	R _h ^d [nm]
1	0	4.96	1.02	10.1	10.1
2	2	5.01	1.01	9.4	9.4
3	5	5.32	1.06	8.4	8.6
4	10	5.45	1.06	7.3	7.9

^a Conditions: solvent = THF, *t* = 16 h, *T* = 35 °C, Ir(I) = [IrCl(COE)₂]₂.

^b Relative to original COD content. ^c Determined by triple-detector SEC in THF. ^d Determined by DLS in THF.

chain collapse at high dilution, treatment of ROMP derived poly(*cis*-cyclooctene) (pCOE) with Ir complex 2 in dilute THF solution did not afford a well-defined organometallic nanoparticle. Instead, an insoluble cross-linked material precipitated from solution, reminiscent of the intermolecular cross-linking observed in the rhodium case.³²

The control of intramolecular chain collapse was also probed by systematically varying the percentage of iridium(I) introduced onto the polymer chain. As in the case of Rh-ONPs, the newly generated Ir-ONPs exhibited a linear dependence between iridium(I) (cross-linker) added and the reduction in the size of the particles. Therefore, upon increasing the metal content from 2 mol% to 10 mol%, a regular decrease in the hydrodynamic radius was observed by both size exclusion chromatography (SEC) and dynamic light scattering (DLS) studies in THF (Fig. 1 and Table 1).

Moreover, UV-Vis spectroscopy was also used to monitor the varying concentrations of Ir(I) in the formation of Ir-ONPs. As expected, a gradual rise in the intensity of the absorption band at 446 nm consistent with the increase of iridium(I) content in the polymer chain was observed (Fig. S26, ESI†).

As shown in Table 1, the hydrodynamic radii obtained by using triple-detector SEC in THF showed excellent correlations with those obtained by DLS measurements. As expected, the intrinsic viscosity was also reduced with increasing amount of metal incorporated into the polymer chain (Fig. S27a, ESI†). For convenience, a plot of the results obtained in the DLS measurement of the hydrodynamic radius *vs.* the iridium content of the ONPs is shown in Fig. 2.

As an additional characterization method for the Ir-ONPs (10 mol% Ir(I)), cryogenic transmission electron microscopy (TEM) analysis was carried out. The spherical particles imaged, of about 20 nm diameter, nicely correlate with the results obtained by DLS and triple-detector SEC (Fig. S28a and b, ESI†). The amount of iridium embedded into the polymer chain was quantified by ICP-MS analysis giving an iridium content of 125 mg g⁻¹ of the pCOD; confirming the successful cross-linking.

Synthesis of organometallic nanoparticles of nickel(0)

Having secured the straightforward synthesis of both Ir-ONPs and Rh-ONPs, we turned our attention to produce pCOD complexes of nickel. Although nickel(0) has been shown to bind 1,5-dienes,³⁶ its complexes are usually less stable compared to the corresponding rhodium(I) and iridium(I)/diene complexes.

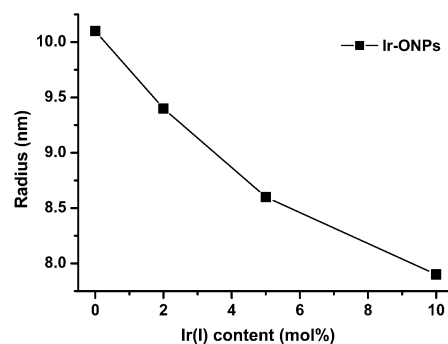
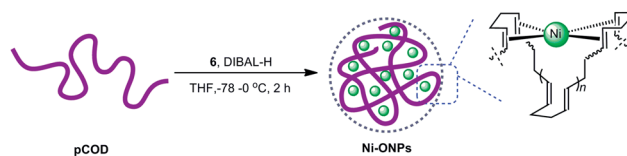


Fig. 2 Plot of hydrodynamic radius (measured by DLS) of Ir-ONPs vs. iridium(I) content.



Scheme 2 Schematic illustration of the synthesis of Ni-ONPs.

This drawback makes the procedures used for rhodium and iridium incompatible for nickel. Thus, nickel(II) acetylacetonate (6) had to be used as the precursor cross-linker to generate the ONP. Auspiciously, the *in situ* reduction of 6 with DIBAL-H in the presence of pCOD afforded the desired Ni-ONPs (Scheme 2).³⁷

Again, the polymer solution was kept highly diluted ($\approx 10^{-5}$ M) in order to avoid any possible intramolecular cross-linking. SEC and DLS measurements revealed the smooth formation of Ni-ONPs showing a systematic reduction in the hydrodynamic radius upon increasing the nickel content in the polymer chain, reproducing the linear dependence found between the amount of metal added and the hydrodynamic radius of the polymer (Fig. 3 and Table 2). Similarly, a reduction in the measured intrinsic viscosity was observed also for Ni-ONPs upon increasing the amount of incorporated metal (Fig. S27b, ESI†).

In contrast to the rhodium and iridium polymer complexes, the Ni-ONPs had to be kept under inert atmosphere in order to avoid decomposition (gradual decomposition was observed over 24 h under air). Nonetheless, these nanoparticles were stable enough to be measured by SEC and DLS analyses.

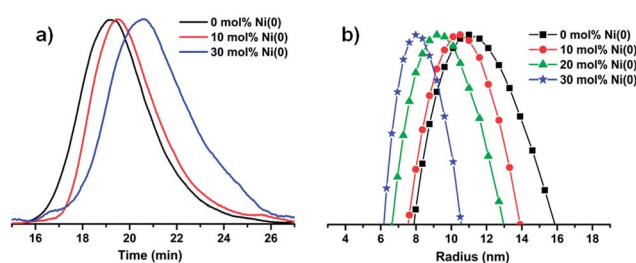
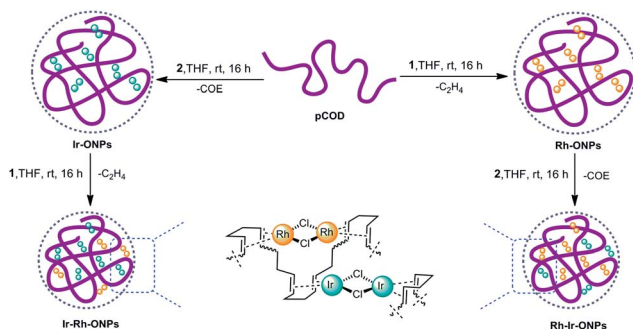


Fig. 3 (a) Overlay of the SEC traces obtained for Ni-ONPs at varying concentrations of Ni(II). (b) Overlay of DLS traces obtained for Ni-ONPs at varying concentrations of Ni(II).

Table 2 SEC and DLS measurements of Ni-ONPs with varying nickel content^a

Entry	Ni(II) ^b [mol%]	M _n ^c [$\times 10^4$ g mol ⁻¹]	PDI	R _h ^d [nm]
1	0	4.40	1.03	10.5
2	10	3.60	1.01	9.6
3	20	3.00	1.05	9.1
4	30	2.55	1.15	8.0

^a Reaction conditions: solvent = THF, $t = 2$ h, $T = -78-0$ °C, Ni(II) = [Ni(acac)₂], DIBAL-H = 2.5 equiv. w.r.t. Ni(II). ^b Relative to original COD content. ^c Determined by triple-detector SEC in THF. ^d Determined by DLS in THF.



Scheme 3 Schematic illustration of the synthesis of organobimetallic ONPs of rhodium(I) and iridium(I) (Rh-Ir-ONPs and Ir-Rh-ONPs).

Synthesis of organobimetallic nanoparticles of rhodium(I) and iridium(I)

The facile procedure by which the addition of metal ions induced the formation of the ONPs persuaded us to attempt the synthesis of bimetallic nanoparticles. Organobimetallic nanoparticles have the enormous potential to achieve cooperative or tandem catalysis, where a single ONP may combine the catalytic efficiency of both embedded metals.³⁸⁻⁴¹

In addition, we surmised that lodging different metals in close proximity, and in any desired ratio, could have implications even beyond catalyst development.

Thus, cross-linkers **1** and **2** were sequentially introduced to a solution of pCOD (Scheme 3). Indeed, bimetallic nanoparticle formation could be ascertained by both SEC and DLS measurements (Fig. 4). For example, the addition of **1** to pCOD reduced the hydrodynamic radius of the parent polymer from 11.0 nm to 9.6 nm, followed by a subsequent reduction to 8.7 nm after the addition of the second complex (**2**) (Table 3).

A comparative kinetic study was conducted for both cross-linkers **1** and **2** using the stopped-flow technique. The analysis showed complete ligand exchange of **1** and **2** with pCOD in less than one minute (Fig. S1, ESI[†]).

To confirm that both metals are actually independently interacting with the polymer, the sequence of cross-linker addition was reversed. Thus, addition of complex **2** to pCOD reduced the hydrodynamic radius of the particles from 11.0 nm to 9.6 nm, which was then decreased to 8.4 nm when complex **1** was added (Table 3).

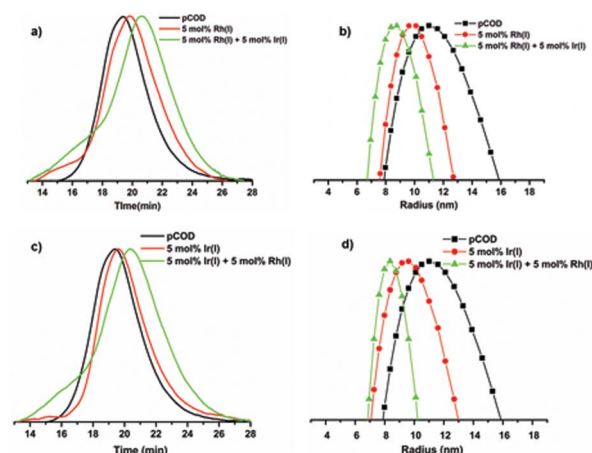


Fig. 4 (a) Overlay of SEC traces obtained for Rh-Ir-ONPs by the addition of 5 mol% Rh(I) followed by 5 mol% Ir(I). (b) Overlay of DLS traces obtained for Rh-Ir-ONPs by the addition of 5 mol% Rh(I) followed by 5 mol% Ir(I). (c) Overlay of SEC traces obtained for Ir-Rh-ONPs by the addition of 5 mol% Ir(I) followed by 5 mol% Rh(I). (d) Overlay of DLS traces for Ir-Rh-ONPs obtained by the addition of 5 mol% Ir(I) followed by 5 mol% Rh(I).

As further evidence for bimetallic ONP formation, the newly generated **Rh-Ir-ONPs** showed absorption maxima corresponding to both Rh/diene and Ir/diene fragments respectively at 368 nm (compared to 365 nm for **Rh-ONPs**) and 443 nm (compared to 446 nm for **Ir-ONPs**), presenting a convenient additional spectroscopic handle for the characterization of these structures (Fig. 5). The formation of bimetallic complexes of pCOD was also monitored by ¹H NMR analyses. The appearance of broad peaks at $\delta = 4.31-4.43$ ppm and $\delta = 4.56-4.72$ ppm corresponding to the olefinic protons bound to Rh and Ir metal centers provides good evidence of complex formation (Fig. S19, ESI[†]). Furthermore, TEM analysis of **Rh-Ir-ONPs** containing 5 mol% rhodium and 5 mol% iridium showed spherical particles of about 20 nm in diameter (Fig. S28c and d, ESI[†]).

Table 3 SEC and DLS measurements of organobimetallic nanoparticles containing rhodium(I) and iridium(I)^a

Entry	Rh(I) ^b [mol%]	Ir(I) ^b [mol%]	M _n ^c [$\times 10^4$ g mol ⁻¹]	PDI	R _h ^d [nm]
pCOD	—	—	5.71	1.02	11.0
Rh-ONPs	2.5	—	4.63	1.01	10.4
	5	—	5.52	1.04	9.6
Rh-Ir-ONPs	2.5	7.5	7.18	1.12	8.7
	5	5	6.05	1.11	8.7
Ir-ONPs	—	2.5	4.20	1.09	10.6
	—	5	4.50	1.07	9.6
Ir-Rh-ONPs	7.5	2.5	7.13	1.11	8.7
	5	5	5.72	1.03	8.4

^a Conditions: solvent = THF, $t = 16$ h, $T = 35$ °C, Rh(I) = [RhCl(C₂H₄)₂]₂, Ir(I) = [IrCl(COE)₂]₂. ^b Relative to original COD content. ^c Determined by triple-detector SEC in THF. ^d Determined by DLS in THF.

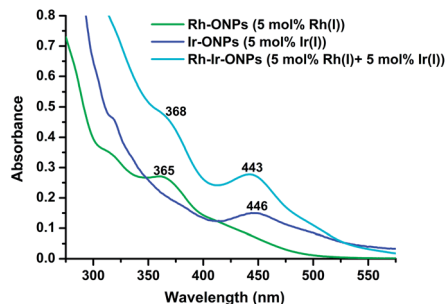


Fig. 5 Overlay of UV-Vis spectra obtained for organobimetallic nanoparticle (Rh-Ir-ONPs), Rh-ONPs and Ir-ONPs.

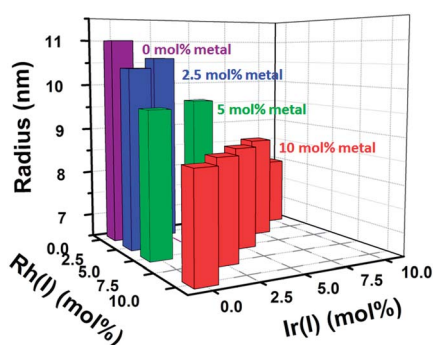


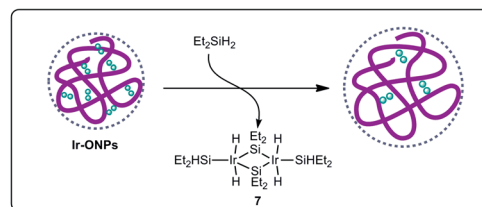
Fig. 6 Plot of hydrodynamic radius against varying ratios of rhodium and iridium.

The final rhodium (34 mg g^{-1}) and iridium (49 mg g^{-1}) contents were quantified by ICP-MS analysis confirming the successful synthesis of the bimetallic ONPs.

Finally, we decided to probe whether different metal ratios could also be used to form ONPs, and what effect this would have on the size of the particle. As observed in Fig. 6, ONPs retained approximately the same dimensions irrespective of the ratio of rhodium and iridium incorporated into the polymer chain, only the total amount of metal dictated the final size. Therefore, one or more metals in any desired ratio can be readily inserted into the polymer chain to achieve both size and composition control.

Preliminary applications of Rh(I) and Ir(I)-ONPs in catalysis

One of the most attractive potential uses for the organometallic nanoparticles is their potential to provide accessible metal ions to the surrounding media for catalytic applications. Thus, the polymer may act as a type of “metal sponge”, releasing active species into solution when the appropriate conditions are met. The use of ONPs for chemical catalysis is expected to offer several advantages. First, unlike dendrimers and other complex macromolecular architectures which often demand lengthy and expensive procedures, these polymer-based systems are inexpensive and may be synthesized very easily under mild reaction conditions. Second, after the reaction, the product could be readily isolated by simple precipitation of the nanoparticles. Most importantly, dense packing of active metal species into the



Scheme 4 Reduction of benzyl benzamide (8) by using Ir-ONPs.

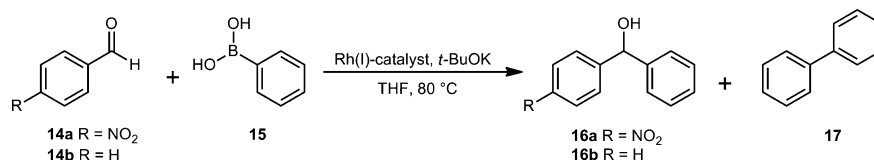
hydrophobic volume of the nanoparticle may bring about unexpected reactivities.

Rhodium and iridium/diene catalysed cross-coupling reactions are well established synthetic methods in organic synthesis,^{42–48} and diene ligands are considered as viable alternatives to phosphines in many important transformations.⁴⁴ Compelled by this notion, we probed the chemical accessibility of iridium(i) in **Ir-ONPs** by mirroring a recently reported reduction of secondary amides by an iridium silane complex (7) (Scheme 4).⁴⁹

In this successful example, the ONPs were employed just as the metal supplier for a known catalytic reaction. Encouraged by this result, we set out to probe the catalytic performance of the **Ir-ONPs** in a reaction where the Ir(I)/1,5-diene moiety remains intact (no detachment of Ir from the ONP is expected). As recently reported by Barker *et al.*,⁴⁶ no catalysis was observed when the iridium complexes were not ligated to dienes in ketone allylations. Thus, this reaction would offer a good assessment for the premise that catalysis must proceed within the ONP space and not by the formation of a freestanding Ir unit in solution. For this purpose, **Ir-ONPs** were tested in a benchmark allylation of acetophenone (Scheme S2, ESI†). Indeed, the allylation reaction of acetophenone (11) with allyl boronic acid pinacol ester (12) in the presence of 2 mol% of **Ir-ONPs** (2 mol% of Ir(I)/1,5-diene units with respect to substrates) smoothly afforded the expected allylated product 13 in 97% yield in 24 h (Table S1, ESI†). After the reaction the **Ir-ONPs** were evaporated, washed and reused three times without losing any of their catalytic activity. The recycled **Ir-ONPs** showed more than 95% conversion even after the third recycling (Table S1, ESI†).

Having shown that the ONPs can carry out reactions with similar efficiency as their small molecule models, we sought to determine whether the peculiar arrangement of metal complexes within the polymer matrix may lead to different catalytic behaviour.

Two factors may influence the reactions catalyzed by the ONPs, the first is that if the reaction is taking place inside the ONP, then the polarity environment will be different than that of the bulk solution. The second factor that may cause reactions to behave differently is that the distribution of the catalytically active metal fragments is not homogeneous throughout the solution because the ions are supposed to be concentrated within the nanoparticle. Thus, 4-nitrobenzaldehyde (14a) and



Scheme 5 Rh(I) mediated cross-coupling reaction between 14 and 15.

Table 4 Cross-coupling reaction of 14 and 15 using Rh(I) catalysts^a

Entry	Catalyst	[Aldehyde] [mmol L ⁻¹]	[Rh(I)] [mmol L ⁻¹]	<i>t</i> [h]	Conv. ^b [%]	16 ^b [%]	17 ^b [%]
1	Rh-ONPs ^c	10.0	0.5	48	40	—	>99
2	18	10.0	0.5	16	>99	>99	—
3	18	10.0	10.0	16	>99	92	8
4	18	3.0	3.0	16	>99	84	16
5	18	2.0	0.1	16	>99	70	30
6	Rh-ONPs ^c	10.0	0.5	48	26	—	>99
7	18	10.0	0.5	16	>99	93	7

^a Conditions: solvent = THF, *T* = 80 °C, boronic acid = 2 equiv. per aldehyde. ^b Determined by GC-MS analysis. ^c Rh(I) = 10 mol% w.r.t the 1,5-hexadiene elements in the polymer chain, aldehyde = 14a (entries 1–5) and 14b (entries 6 and 7).

phenyl boronic acid (15) were chosen as the standard coupling partners (Scheme 5). The results of the cross-coupling reactions employing Rh-ONPs and the control reactions using isolated complex [RhCl(COD)]₂ (18) at different reaction conditions are detailed in Table 4. The reaction using 5 mol% of 18 resulted in the complete conversion of the starting materials to the expected cross-coupled product 16a (Table 4, entry 2). In contrast, the reaction using Rh-ONPs gave moderate conversions and a negligible yield of cross-coupled product (Table 4, entry 1). Interestingly, the major product formed in this case was biphenyl.^{50,51} In order to understand the underlying mechanism, various control reactions were carried out. We assumed that the higher effective concentration of Rh(I)/diene within the ONPs might play a role in the outcome of the reaction. Indeed, by simply raising the concentration of 18, a larger amount of biphenyl was produced (Table 4, entry 3).

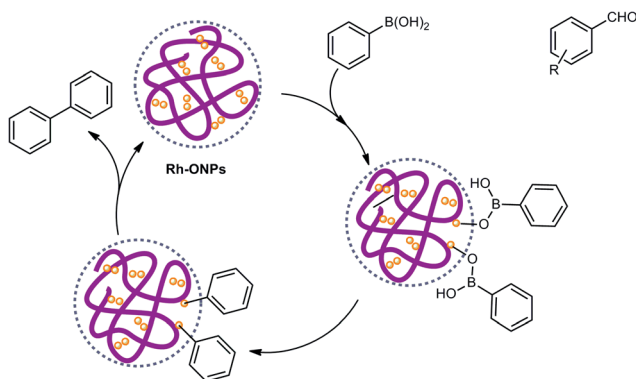
Moreover, when the reaction was performed under more dilute conditions, maintaining an equimolar ratio of substrate to catalyst, the amount of biphenyl formed was even higher

(Table 4, entry 4). The amount of biphenyl formation could be further increased from 16% to 30% (Table 4, entry 5) when the standard reaction ratios (*i.e.*, using 5 mol% catalyst relative to aldehyde) were kept and the reaction was carried out under high dilution (5 times); maybe simulating events that occur in a nanoparticle where the rhodium quickly reacts with boronic acid and does not have a significant effective concentration of aldehyde in the surroundings. These results support a view where the homo-coupling reaction is occurring either within or on the surface of the ONPs, where the effective concentration of Rh(I)/diene is much higher than in the neighboring environment (Scheme 6). In order to probe whether the highly non-polar nature of the ONPs might be the cause for the observed behaviour, a less polar aldehyde, 14b, was used instead of 14a. However, biphenyl was still the only product observed (Table 4, entry 6) and the conversion was even lower. In contrast, the control reaction using complex 18 afforded cross-coupled product 16b as the major product (Table 4, entry 7).

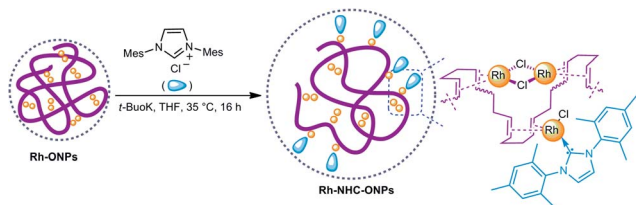
Although similar types of homo-coupling have been reported elsewhere in the literature,⁵² selective homo-couplings under conditions favorable to cross-coupling have not been reported. This alluring property of ONPs may have a significant impact on the outcome of other ONP catalyzed reactions and we plan to continue to study this outstanding behaviour.

Since formation of biphenyl was observed with a closely packed Rh(I) environment within the nanoparticle, we asked ourselves whether partial unfolding of ONPs by the introduction of coordinating NHCs could shift the catalytic outcome of the ONPs from homo- to cross-coupling.

Transition metal complexes bearing N-heterocyclic carbenes (NHCs) have had an enormous impact in organic synthesis.^{53,54} Chaudret *et al.* have recently shown a very nice example of how NHCs can influence the formation and properties of metallic nanoparticles.⁵⁵



Scheme 6 Schematic proposal for the biphenyl production catalysed by Rh-ONPs.



Scheme 7 Preparation of Rh-ONPs bearing NHCs.

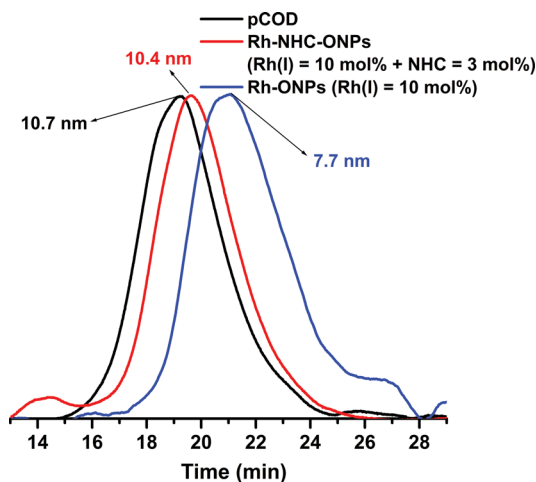


Fig. 7 SEC overlay of pCOD, Rh-ONPs and Rh-NHC-ONPs bearing 3 mol% NHC.

In general, NHC complexes may be easily obtained by ligand exchange processes.⁵⁶ Within the ONP, the introduction of NHC ligands would be expected to replace a diene-metal bond and change the electronic environment of the metal and increase the polymer size (Scheme 7).

For this purpose, 3 mol% (with respect to the 1,5-hexadiene elements in the polymer chain) 1,3-bis(2,4,6-trimethylphenyl)imidazolium chloride was mixed with the **Rh-ONPs** containing 10 mol% of Rh(I) and potassium *tert*-butoxide was added to generate the NHC *in situ*. Indeed, the introduction of an NHC ligand led to a significant increase in size, probably because of the relatively large size of the NHC (Fig. 7) in addition to the severance of a cross-linking bond.

Having shown that the introduction of NHC ligands led to less compact ONPs, the cross-coupling reaction of **14a** and **15** was repeated using NHC containing **Rh-ONPs** as catalysts (**Rh-**

Table 5 Cross-coupling reaction of **14a** and **15** using Rh-NHC-ONPs as catalyst^a

Entry	Catalyst	Rh(I) ^b [mol%]	NHC ^b [mol%]	16a ^c [%]	17 ^c [%]
1	Rh-ONPs	10	0	—	>99
2	Rh-NHC-ONPs	10	3	19	81
3	Rh-NHC-ONPs	10	10	70	30
4	18	—	—	>99	—

^a Conditions: solvent = THF, $T = 80\text{ }^{\circ}\text{C}$, catalyst = 5 mol%. ^b Rh(I) = 10 mol% w.r.t. the 1,5-hexadiene elements in the polymer chain.

^c Determined by GC-MS analysis.

NHC-ONPs) (Table 5). Notably, a substantial improvement in the formation of cross-coupled product was observed (Table 5, entry 2). Moreover, complete unfolding of the ONP by using stoichiometric amounts of NHC (with respect to the metal) further improved the selectivity to achieve 70% cross-coupled product (Table 5, entry 3) (naturally, the rhodium is still attached to the polymer, but does not cross-link it as it only needs one diene ligand).

In brief, the catalytic activity of the ONP could be switched in a controlled manner *via* the addition of NHC ligands.

Conclusions

We have shown that the synthesis of organometallic nanoparticles based on ROMP derived pCOD may be readily extended to other transition metals. The ONPs were fully characterized by SEC, DLS and TEM analyses. The sizes of all ONPs could be controlled by the amount of cross-linking metal complex added and the formation of the new metal-polymer hybrids could be established by simple UV-Vis spectroscopy measurements. Moreover, the facile and mild synthetic procedures allow also for the generation of nanoparticles containing more than one metal in any desired ratio. The associative character of the bimetallic ONP formation process strongly suggests that the metals are randomly distributed within the polymer framework, although no direct evidence of the spatial distribution of the metals within the ONPs could be obtained until now. We surmise, based on our findings, that any metal that can bind to 1,5-cyclooctadiene has the potential ability to be incorporated into these pCOD nanoparticle frameworks. The ONPs synthesized were found to be catalytically active in several reactions, and we showed that the crowded ONP environment gives rise to novel catalytic performance. Research efforts are ongoing to advance tandem/cooperative catalytic methods with the bimetallic ONPs, study the bulk electronic properties of different ONPs with different metals, as well as making use of block copolymers to enhance the stability of these novel materials in other solvents.

Acknowledgements

The United States-Israel Binational Science Foundation (2010047) is acknowledged for partial funding of this study. The authors thank Dr Sharon Vanounou and Dr Yael Levi-Kalishman (Ilse-Katz Institute for Meso- and Nano-scale Science and Technology, Ben-Gurion University of the Negev) for technical assistance in dynamic light scattering data analysis and TEM imaging. We also wish to thank Dr Alexandra Massarwa for assistance with the stopped-flow instrument and Dr Sarit Yerushalmi for assistance with ICP-MS measurements.

Notes and references

- 1 C. Slugovc, *Macromol. Rapid Commun.*, 2004, **25**, 1283.
- 2 P. J. M. Stals, Y. Li, J. Burdyńska, R. Nicolaÿ, A. Nese, A. R. A. Palmans, E. W. Meijer, K. Matyjaszewski and S. S. Sheiko, *J. Am. Chem. Soc.*, 2013, **135**, 11421.

- 3 J.-S. Wang and K. Matyjaszewski, *J. Am. Chem. Soc.*, 1995, **117**, 5614.
- 4 V. C. Gibson, *Adv. Mater.*, 1994, **6**, 37.
- 5 A. Leitgeb, J. Wappel and C. Slugovec, *Polymer*, 2010, **51**, 2927–2946.
- 6 S. Sutthasupa, M. Shiotsuki and F. Sanda, *Polym. J.*, 2010, **42**, 905–915.
- 7 G. R. Whittell, M. D. Hager, U. S. Schubert and I. Manners, *Nat. Mater.*, 2011, **10**, 176–188.
- 8 E. M. Natanson and M. T. Bryk, *Usp. Khim.*, 1972, **41**, 1465–1493.
- 9 J. M. Calvert and T. J. Meyer, *Inorg. Chem.*, 1981, **20**, 27.
- 10 M. Ramanathan and S. B. Darling, *Polymer Int.*, 2013, **62**, 1123.
- 11 C. Ulbricht, C. R. Becer, A. Winter and U. S. Schubert, *Macromol. Rapid Commun.*, 2010, **31**, 827.
- 12 M. Burnworth, L. Tang, J. R. Kumpfer, A. J. Duncan, F. L. Beyer, G. L. Fiore, S. J. Rowan and C. Weder, *Nature*, 2011, **472**, 334–338.
- 13 P. D. Zeits, T. Fiedler and J. A. Gladysz, *Chem. Commun.*, 2012, **48**, 7925.
- 14 V. A. Du and I. Manners, *Macromolecules*, 2013, **46**, 4742.
- 15 D. E. Bergbreiter, *Chem. Rev.*, 2002, **102**, 3345–3384.
- 16 N. E. Leadbeater and M. Marco, *Chem. Rev.*, 2002, **102**, 3217–3274.
- 17 D. E. Bergbreiter, J. Tian and C. Hongfa, *Chem. Rev.*, 2009, **109**, 530–582.
- 18 R. Wang and Z.-G. Wang, *Macromolecules*, 2014, **47**, 4094.
- 19 K. Takeda, T. Oohara, M. Anada, H. Nambu and S. Hashimoto, *Angew. Chem., Int. Ed.*, 2010, **49**, 6979–6983.
- 20 N. Kann, *Molecules*, 2010, **15**, 6306–6331.
- 21 M. A. J. Gillissen, T. Terashima, E. W. Meijer, A. R. A. Palmans and I. K. Voets, *Macromolecules*, 2013, **46**, 4120.
- 22 (a) M. Aiertza, I. Odriozola, G. Cabañero, H.-J. Grande and I. Loinaz, *Cell. Mol. Life Sci.*, 2012, **69**, 337; (b) A. Sanchez-Sanchez, I. Perez-Baena and J. A. Pomposo, *Molecules*, 2013, **18**, 3339.
- 23 G. Allen, J. Burgess, S. F. Edwards and D. J. Walsh, *Proc. R. Soc. London, Ser. A*, 1973, **334**, 453.
- 24 J. E. Martin and B. E. Eichinger, *Macromolecules*, 1983, **16**, 1345.
- 25 E. Harth, B. V. Horn, V. Y. Lee, D. S. Germack, C. P. Gonzales, R. D. Miller and C. J. Hawker, *J. Am. Chem. Soc.*, 2002, **124**, 8653.
- 26 S. C. Zimmerman, M. S. Wendland, N. A. Rakow, I. Zharov and K. S. Suslick, *Nature*, 2002, **418**, 399–403.
- 27 A. E. Cherian, F. C. Sun, S. S. Sheiko and G. W. Coates, *J. Am. Chem. Soc.*, 2007, **129**, 11350.
- 28 N. G. Lemcoff, T. A. Spurlin, A. A. Gewirth, S. C. Zimmerman, J. B. Beil, S. L. Elmer and H. G. Vandever, *J. Am. Chem. Soc.*, 2004, **126**, 11420–11421.
- 29 E. A. Appel, J. Dyson, J. del Barrio, Z. Walsh and O. A. Scherman, *Angew. Chem., Int. Ed.*, 2012, **51**, 4185.
- 30 B. Zhu, G. Qian, Y. Xiao, S. Deng, M. Wang and A. Hu, *J. Polym. Sci., Part A: Polym. Chem.*, 2011, **49**, 5330.
- 31 J. B. Beck, K. L. Killops, T. Kang, K. Sivanandan, A. Bayles, M. E. Mackay, K. L. Wooley and C. J. Hawker, *Macromolecules*, 2009, **42**, 5629.
- 32 S. Mavila, C. E. Diesendruck, S. Linde, L. Amir, R. Shikler and N. G. Lemcoff, *Angew. Chem., Int. Ed.*, 2013, **52**, 5767.
- 33 A. L. Onderdelinden and A. van der Ent, *Inorg. Chim. Acta*, 1972, **6**, 420–426.
- 34 R. A. Epstein, G. L. Geoffroy, M. E. Keeney and W. R. Mason, *Inorg. Chem.*, 1979, **18**, 478.
- 35 A. M. Striegel, Size-Exclusion Chromatography, in *Liquid Chromatography: Fundamentals and Instrumentation*, ed. S. Fanali, P. R. Haddad, C. Poole, P. Schoenmakers and D. K. Lloyd, Elsevier: Waltham, USA, 2013, ch. 9, pp. 193–223.
- 36 B. Bogdanović, M. Kröner and G. Wilke, *Justus Liebig's Ann. Chem.*, 1966, **699**, 1.
- 37 D. J. Krysan and P. B. Mackenzie, *J. Org. Chem.*, 1990, **55**, 4229.
- 38 J. A. Mata, F. E. Hahn and E. Peris, *Chem. Sci.*, 2014, **5**, 1723.
- 39 C. A. Denard, H. Huang, M. J. Bartlett, L. Lu, Y. Tan, H. Zhao and J. F. Hartwig, *Angew. Chem., Int. Ed.*, 2014, **53**, 465.
- 40 K. Engström, E. V. Johnston, O. Verho, K. P. J. Gustafson, M. Shakeri, C.-W. Tai and J.-E. Bäckvall, *Angew. Chem., Int. Ed.*, 2013, **52**, 14006.
- 41 X. Peng, Q. Pan and G. L. Rempel, *Chem. Soc. Rev.*, 2008, **37**, 1619.
- 42 C. Defieber, H. Grützmacher and E. M. Carreira, *Angew. Chem., Int. Ed.*, 2008, **47**, 4482.
- 43 C. Fischer, C. Defieber, T. Suzuki and E. M. Carreira, *J. Am. Chem. Soc.*, 2004, **126**, 1628.
- 44 F. Glorius, *Angew. Chem., Int. Ed.*, 2004, **43**, 3364.
- 45 J. B. Johnson and T. Rovis, *Angew. Chem., Int. Ed.*, 2008, **47**, 840.
- 46 T. J. Barker and E. R. Jarvo, *Org. Lett.*, 2009, **11**, 1047.
- 47 S. E. Denmark and J. Fu, *Chem. Rev.*, 2003, **103**, 2763.
- 48 T. Hayashi and K. Yamasaki, *Chem. Rev.*, 2003, **103**, 2829.
- 49 C. Cheng and M. Brookhart, *J. Am. Chem. Soc.*, 2012, **134**, 11304.
- 50 T. Vogler and A. Studer, *Adv. Synth. Catal.*, 2008, **350**, 1963.
- 51 A. Lei and X. Zhang, *Tetrahedron Lett.*, 2002, **43**, 2525–2528.
- 52 For a recent example of biphenyl formation from phenylboronic acid see: M. Palashuddin Sk, C. K. Jana and A. Chattopadhyay, *Chem. Commun.*, 2013, **49**, 8235–8237.
- 53 W. A. Herrmann, *Angew. Chem., Int. Ed.*, 2002, **41**, 1290.
- 54 S. Díez-González, N. Marion and S. P. Nolan, *Chem. Rev.*, 2009, **109**, 3612.
- 55 P. Lara, O. Rivada-Wheelaghan, S. Conejero, R. Poteau, K. Philippot and B. Chaudret, *Angew. Chem., Int. Ed.*, 2011, **50**, 12080.
- 56 F. E. Hahn and M. C. Jahnke, *Angew. Chem., Int. Ed.*, 2008, **47**, 3122–3172.